A&A 370, 513–523 (2001)
DOI: 10.1051/0004-6361:20010262

Astronomy & Astrophysics

Turbulent outflows from [WC]-type nuclei of planetary nebulae⋆

II. The [WC 8] central star of NGC 40

Y. Grosdidier[1,2,3,⋆⋆], A. Acker[1], and A. F. J. Moffat[2,3,⋆⋆⋆]

[1] Observatoire Astronomique de Strasbourg, UMR 7550, 11 rue de l'Université, 67000 Strasbourg, France
e-mail: acker@newb6.u-strasbg.fr
[2] Université de Montréal, Département de Physique, CP 6128, Succursale Centre-Ville, Montréal (Québec) H3C 3J7, Canada
e-mail: moffat@astro.umontreal.ca
[3] Observatoire du mont Mégantic, Canada

Received 19 October 2000 / Accepted 13 February 2001

Abstract. Using spectroscopic observations taken at the Observatoire de Haute-Provence (France) and the Observatoire du mont Mégantic (Canada), we describe wind fluctuations in the [WC 8]-type central star of the planetary nebula NGC 40, HD 826, which was observed intensively during 22 nights. Moving features seen on the top of the C IIIλ5696 and C IV$\lambda\lambda$5801/12 (+C IIIλ5826) emission lines are interpreted as outflowing "blobs" which are radially accelerated outwards in the Wolf-Rayet wind. The amplitudes of the variations range up to 25–30% of the adjacent continuum flux, over timescales of hours. The variabilities of both lines are quite well correlated, although they are somewhat weaker for the C IV complex. Subpeaks (or gaps) on the top of the C III line generally move towards the nearest line edge in a symmetric fashion in the blue and the red. Kinematic parameters of the blobs were derived and compared to those observed for massive and other low-mass Wolf-Rayet stars. Especially impressive are the significantly larger observed maximum radial acceleration values of the blobs, compared to those already reported for massive WC 5–9, or low-mass [WC 9] stars. This is attributed to the very small stellar radius of HD 826. In addition the β velocity field is found to possibly underestimate the true gradient within the stellar wind flow. On the whole, the wind of HD 826 is highly stochastically variable on a very short time-scale. This supports a turbulent origin.

Key words. stars: individual: HD 826 – planetary nebulae: individual: NGC 40 – stars: mass-loss – stars: atmospheres – stars: Wolf-Rayet – turbulence

1. Introduction

1.1. Central stars of planetary nebulae showing the Wolf-Rayet phenomenon

It is well known that the Wolf-Rayet (WR) phenomenon is not restricted to bright, massive stars, but that it is also found among the central stars of some (≈50) planetary nebulae (PN), the so-called [WC] stars (Acker et al. 1992; Tylenda et al. 1993; Peña et al. 1998). About twenty percent (van der Hucht 1996; van der Hucht 1999) of the known stars showing the WR phenomenon in our Galaxy are central stars of PN. All the PN nuclei exhibiting a WR spectrum belong to the WC sequence (Tylenda et al. 1993), and appear virtually hydrogen free. No WN-type central star is known now that M 1-67 (= Sh 2-80), surrounding WR 124 (Spectral type: WN 8), has been removed from the list of bona-fide PN (Crawford & Barlow 1991).

The similarities in line profiles suggests that the winds of [WC] central stars are scale models of the winds of the massive WC stars. However, the level of excitation conditions among WR central stars is quite different since it spans a large range, from [WC 2] to [WC 11] (Méndez & Niemela 1982; Hu & Bibo 1990; van der Hucht 1996), compared to WC 4–WC 9 (with extension to WO 1–WO 5 at the hot-end) for massive, Population I WR stars

Send offprint requests to: Y. Grosdidier,
e-mail: yves@ll.iac.es

⋆ Based on observations taken at the Observatoire de Haute-Provence, France, and at the Observatoire du mont Mégantic, Canada.

⋆⋆ *Present address:* Instituto de Astrofísica de Canarias, Calle Vía Láctea s/n, 38200 La Laguna, Spain.

⋆⋆⋆ Killam Fellow of the Canada Council for the Arts.

(van der Hucht 1996). Note that such an extended distribution of spectral types (although the [WC 5–7] subtypes are apparently less represented; Acker et al. 1996; van der Hucht 1996) may additionally provide a *broad* baseline for comparison and detection of overall trends that otherwise might be drowned out in data generally showing large intrinsic dispersions within a given spectral type.

Although the loss of the outer hydrogen-rich envelope appears to be a necessary condition to the onset of the WR phenomenon, it is clearly not a sufficient one: the large majority of PN central stars (≈50 of ≈350 central stars for which the spectrum is known) does not have a WR-like spectrum (Acker et al. 1992). We still do not know *exactly* what determines some PN central stars to become [WC] stars. Moreover, the observational data, despite their incompleteness or low accuracy for many [WC] central stars, suggest that what distinguishes a [WC] star is not its present physical properties (Acker et al. 1996; Pottasch 1996), but rather more likely its initial properties and evolutionary history. This complicates the study of their precise origin. However, the status and evolutionary history of the PN central stars, as well as their ultimate fate as white dwarfs, is somewhat better known than that of their massive counterparts. The latter point combined with the broad range of excitation conditions of the nuclei suggests that [WC] central stars may facilitate understanding the WR phenomenon as a whole.

1.2. Fragmented, hot star winds; probing the turbulent structure of [WC] winds

Moving subpeaks are systematically seen on the tops of broad optical emission lines from massive WR stars (Robert 1992; Lépine & Moffat 1999, and references therein). These subpeaks suggest WR winds are *inhomogeneous* and *non-stationary* on a time-scale of hours. Eversberg et al. (1998) have also reported stochastic, variable substructures in the He IIλ4686 emission line originating in one O supergiant star. The latter study points to the likely *universal* nature of wind clumping originating in massive, hot stars.

In Grosdidier et al. (2000; hereafter Paper I), wind fluctuations were described for four [WC 9–10] stars, including BD +30°3639 ([WC 9]) observed intensively during 15 nights. In the latter study, the authors show that the wind clumping originating in BD +30°3639 is remarkably similar to that reported for one of its massive, WC 9 counterparts, WR 103. Therefore, they interpreted this fact as strong evidence for understanding the WR phenomenon as a purely atmospheric phenomenon independent of the differences between massive and low-mass WR stars. The present paper will discuss the case of the hotter subtype [WC 8]. The case of the cooler subtypes, [WC 10–12], will be investigated in detail in future studies.

In order to resolve the narrow subpeaks present on the tops of the emission lines originating in BD +30°3639 ([WC 9]), Grosdidier et al. (Paper I) and Acker et al. (1997) found it necessary to have a spectral resolution of about one Angström, or better. For NGC 40, the Balick et al. (1996) spectroscopic data and our first observations (January 96; see Sect. 2 for details) demonstrated to us that a 3 Å spectral resolution is sufficient. Since the subpeaks are very weak, securing time resolution along with sufficient S/N ratio imposes the use of large telescopes. As a compromise, one has to concentrate on relatively bright [WC] central stars observed intensively, especially when using 2 m class telescopes, as in the present study.

Some 17 [WC]-late ([WC 8–12]) central stars are known within the Galaxy (Górny & Stasińska 1995; Acker, private communication) and only two belong to the [WC 8] spectral type. The [WC 8] nucleus of M 2-43 (= PN G027.6+04.2) is certainly too faint ($V \approx 15.7$) for our project. Therefore, the central star of NGC 40, HD 826, which is 4.1 mag brighter in the visible domain ($V \approx 11.6$), appears obviously to be the best target for studying [WC 8] spectroscopic flickering. We concentrated our intensive spectroscopic program on the C IIIλ5696 and C IV$\lambda\lambda$5801/12+C IIIλ5826 emission lines originating in HD 826 observed intensively during 22 nights with 2 m class telescopes. Because they are relatively bright and have comparable intensities in [WC 8] stars, they are the best lines to study expanding stellar wind variability in the optical domain. In addition, the blend-free C IIIλ5696 emission line constitutes an excellent line to trace the movements of independent subpeaks, which are blurred by mixing in the adjacent blended C IV$\lambda\lambda$5801/12+C IIIλ5826 emission line.

1.3. The [WC 8] central star of the planetary nebula NGC 40: HD 826

The PN NGC 40 is a well known nebula, with a 48″-diameter barrel-shaped core, surrounded by two haloes; a faint, diffuse, inner halo out to 90″, and an outer halo with jet-like structures extending to 4′; see Meaburn et al. (1996). These authors noted that turbulent motions exist in the nebula, an observation confirmed by the analysis of nebular line profiles (Neiner et al. 2000). NGC 40 is unusual, because the low excitation class ($p = 1$) of the nebula suggests a stellar temperature of about 30 000 K, whereas the UV spectrum of the nucleus is compatible with a temperature three times higher. This discrepancy can be explained by the existence of a "carbon curtain" in the nebula (Bianchi & Grewing 1987). C IIλ6578 emission was observed to be coincident with the 48″ [N II] shell, implying that the expanding central envelope is relatively rich in carbon (see Meaburn et al. 1996). The PN NGC 40 probably originated from a relatively massive progenitor (6 $M_\odot$; Bianchi 1992).

The effective temperature of HD 826 was estimated at 46 000 K by Leuenhagen et al. (1996), although some authors report effective temperatures as low as 30 000 K (Köppen & Tarafdar 1978), or as high as 90 000 K

Table 1. Log of spectroscopic observations of NGC 40's central star. The exposure times were 1000 s (OMM) and 1800 s (OHP)

Denomination	**Central star**		**Journal**	**of**	**observations**	
PNG	Spectr. type	Telescope (diam.)	Spectr. range	S/N	Date	No. of
Usual name PN	V^a	Spectrograph	Resol. power (RP)			spectra
Star name						
(1)	(2)	(3)	(4)	(5)	(6)	(7)
120.0+09.8	[WC 8]	OMM (1.6 m)	5300–5960 Å	78	1996 Jan. 11	12
NGC 40	11.6	B&C	≈2.8 Å (2000)	48	1996 Jan. 15	22
HD 826				44	1996 May 26	15
				42	1996 May 27	15
				40	1996 May 30	13
				80	1996 Jul. 28	18
				56	1996 Sep. 26	26
				65	1996 Sep. 30	19
				43	1996 Nov. 16	34
				63	1996 Nov. 17	32
		OHP (1.52 m)	5250–6000 Å	36	1997 Jan. 12	20
		AURELIE	≈1.1 Å (5000)	39	1997 Jan. 13	19
				26	1997 Mar. 3	8
				21	1997 Mar. 5	13
				16	1997 Mar. 6	12
				29	1997 Mar. 7	14
				7	1998 Jan. 20	5
				17	1998 Jan. 21	18
				19	1998 Jan. 22	19
				17	1998 Jan. 23	17
				20	1998 Jan. 24	12
				18	1998 Jan. 25	9

[a] From the Acker et al. (1992) catalogue.
[b] Characteristic signal-to-noise ratio evaluated in the continuum adjacent to C IIIλ5696.

(Schmutz et al. 1989; Bianchi & Grewing 1987). Using IUE data, Bianchi & Grewing (1987) reported a terminal velocity of 1800 km s^{-1} and a luminosity of 26 200 $L_\odot$. From these results they inferred a radius of 0.66 $R_\odot$ for the continuum-emitting region. Earlier UV spectroscopic data obtained by Benvenuti et al. (1982) led to an even larger terminal velocity, $v_\infty \approx 2370$ km s^{-1}. However, such a value is not reliable because of the poor spectral resolution of their instrumentation. Recent, reliable modelling of the expanding atmosphere (Leuenhagen et al. 1996) led to about 1000 km s^{-1} for the terminal velocity and 0.33 $R_\odot$ for the stellar core radius. PN nucleus spectroscopic flickering similar to that observed for massive WR stars was reported for the first times by Balick et al. (1996) and Grosdidier et al. (1997). They found that the [WC 8] central star of HD 826 shows *fast* moving subpeaks on the top of its flat-topped C IIIλ5696 emission line. Balick et al. (1996) also reported a nearly similar apparent acceleration for all features, the acceleration zone being at least 5 $R_\odot$ in extension.

2. Observations and data reduction

Table 1 gives a log of the spectroscopic observations of HD 826: in Col. (1) the PN and central star designations of NGC 40 are given; in Col. (2) the spectral type and V magnitude of HD 826; in Col. (3) the telescopes and spectrographs used; in Col. (4) the observed spectral range, the adopted spectral resolution and resolving power; in Col. (5) the continuum signal-to-noise ratios for each night given in Col. (6); in Col. (6) the dates of observation; in Col. (7) the number of consecutive spectra acquired each night.

We used the 1.52 m telescope at the Observatoire de Haute-Provence (OHP, France) equipped with the Aurélie spectrograph (see Gillet et al. 1994). The detector was

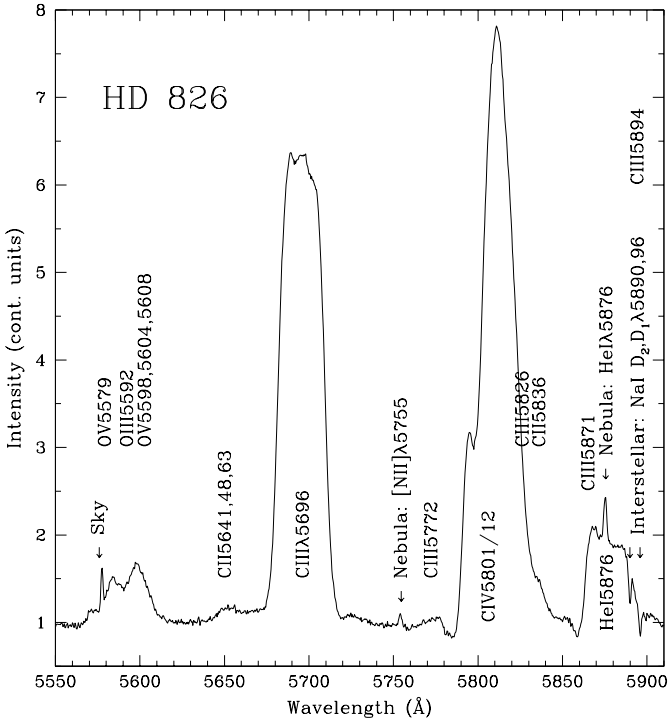

Fig. 1. HD 826 typical normalized spectrum indicating the most obvious emission or absorption features (1998 January 23)

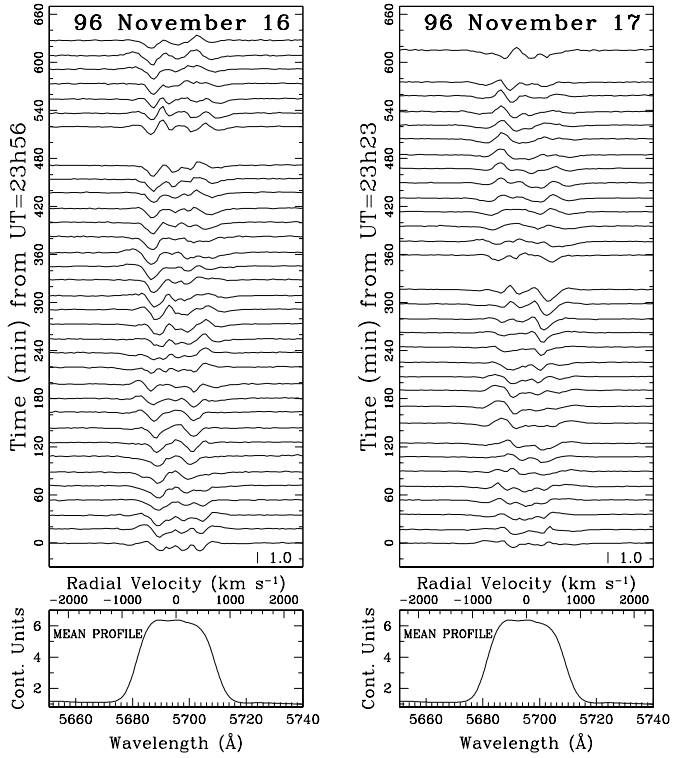

Fig. 2. Residuals from the mean of C IIIλ5696 in HD 826 for 1996 November, 16 and 17. The mean was calculated based on all 22 nights of data. The segment in the lower right corner of the upper panel indicates the amplitude for 1.0 continuum unit in the residuals. Velocities are given relative to $\lambda_0 = 5695.3$ Å. The mean profile in the bottom panels is based on all the spectra in 22 nights

a double linear array Thomson TH7832 of 2048 pixels (Gillet et al. 1994). We used a 300 l/mm grating, leading to a 2.8-pixel resolving power of 5000 (≈1 Å spectral resolution at 5500 Å). The spectral range was centered on 5625 Å and covered 5250–6000 Å. The entrance aperture of Aurélie is circular with a diametre of 3″. We also used the 1.6 m Ritchey-Chrétien, Boller & Chivens telescope at the Observatoire du mont Mégantic (OMM, Canada) combined with the Perkin-Elmer (model 31523) spectrograph at the $f/8$ focus. The detector was a THX CCD with 1024×1024 pixels (before 1996 July 29), or a Loral CCD with 2048×2048 pixels (starting on 1996 September 26). We used a 600 l/mm grating as dispersive element, leading to a 2.2-pixel resolving power of 2000 (≈2.8 Å spectral resolution at 5700 Å). The spectral range, centered on 5630 Å, covered 5300–5960 Å. The width of the slit was 2.5″.

Tests at higher resolutions (0.5 Å and less) were conducted at the OHP (23 spectra taken in January and March 96). At high spectral resolutions, we were forced to significantly increase the exposure times in order to reveal the subpeaks (hence losing time resolution). However, despite longer exposures times (about one hour and more), we only achieved poor S/N ratios precluding any detailed statement concerning the appearance of subpeaks observed at different resolutions. The spectra were reduced in the way described in Paper I with the MIDAS[1] package (OHP data) and the IRAF[2] package (OMM data).

3. Results

Several kinds of features are visible in the observed spectra: i) Broad emission features formed in the stellar wind. The lines of He , C and O are broadened due to the global motion of the expanding stellar wind. Some of the emissions are accompanied by blue-shifted absorption troughs (P-Cygni profiles); ii) Narrow [N II] and He I emission lines which are formed in the planetary nebula. These emission features appear here very weak given the small size of the used apertures and the relatively short exposure times (note that the dimmest parts of NGC 40 are mainly located close to the central star); iii) Interstellar Na I absorption features. See Fig. 1. The rest of this paper will concentrate on i) and their variability.

[1] `http://www.eso.org/projects/esomidas/`

[2] IRAF is distributed by the National Optical Astronomy Observatories, operated by the Association of Universities for Research in Astronomy, Inc., under cooperative agreement with the National Science Foundation. `http://iraf.tuc.noao.edu/`

3.1. Line profile variations

Among the broad emission features in our spectra, the C IIIλ5696 line and the C IV$\lambda\lambda$5801/12+C IIIλ5826 blend dominate in strength and hence merit more intense study. In particular, the C IIIλ5696 line is known to be particularly sensitive to changes in density (e.g. D. J. Hillier, priv. comm.). In Fig. 2, differences from the mean profile (calculated from the whole set of spectra obtained in 22 nights; see lower panels) of the C IIIλ5696 emission line are shown as a function of time for two typical observing nights at the OMM (upper panels). The mean profile in the bottom panel refers to the global mean profile from all 22 nights for this star. In order to reveal the precise appearance of the moving blobs, it is necessary to subtract the smoothest mean profile as possible. For that purpose, we favor the use of the 22-night global mean profile (rather than the nightly mean). The segment in the lower right corner of the upper panel indicates the amplitude for 1.0 continuum unit in the residuals. This amplitude does not take into account the increased variability due to Poisson statistics as the intensity changes across the emission line relative to the adjacent continuum. True amplitudes relative to the continuum will be estimated in Sect. 3.2.

The characteristic time scale for significant variations is confirmed to be a few hours. Ejection times and starting wavelengths of individual blobs appear at random (this will be clearer by inspecting Fig. 6 in a subsequent section). The strongest, most obvious features appear to last longer and move throughout the C III line with *apparently* constant acceleration (see Sect. 3.3).

In order to emphasize the trajectories of subpeaks on the top of the C IIIλ5696 line, Fig. 3 shows grayscale plots of nightly differences from the global mean profile for the 22 nights, which is presented in the lower panels. These plots were obtained in a manner similar to that presented in Paper I. Gaps within the time series appear as a black horizontal bar. In these plots, we also show the trajectories of subpeaks on the top of the nearby C IV$\lambda\lambda$5801/12 emission line. In this complex carbon line, moving subpeaks appear with ghost images on their side. This is likely due to the line blending within this emission line. Unfortunately, the blending of the C IV$\lambda\lambda$5801/12 (+C IIIλ5826) emission feature prevents us from clearly identifying moving features. On the other (weak) lines, the situation is even worse; most of the subpeaks arising from noise can be erroneously associated with true manifestations of local overdensities because of the low S/N ratios in the lines.

3.2. Level of variability

The precise characterization of the variations showed in Figs. 2 and 3 could be greatly influenced by photon statistics and other sources of error. In order to rigorously estimate the significance level of the line profile variations, we have applied the "temporal variance spectrum" analysis (TVS) of Fullerton et al. (1996). For details, we refer the reader to Fullerton et al.'s original paper and to Grosdidier et al. (2000; Paper I). Roughly speaking, the values of the TVS give a statistical assessment of the variability level at a given wavelength. Another outcome of this technique is the possibility of comparing time series of spectroscopic data obtained with different instrumentation and/or inhomogeneous quality.

The temporal variance spectra have been calculated for each of the 21 nights made up of at least 8 individual spectra, in order to secure statistical significance. Figures 4 and 5 have been obtained in the way described in Paper I: they show the related $\mathrm{TVS}^{1/2}$ (i.e. reflecting the amplitude of variability rather than the variance) along with contour levels for significant variability at the 1% and 5% levels. To facilitate the identification of the variable zones, the nightly mean spectra are superposed. The main results are the following:

1. All *obvious* stellar emission lines within our spectral range are variable at the 1% level;
2. In the case of the faint C II$\lambda\lambda\lambda$5641, 48, 63 stellar emission complex, we report only one significant intensification of the activity on 1996 January 15 (up to about 4% of the adjacent continuum flux);
3. The stellar oxygen complex at ≈5590 Å (O Vλ5579, O IIIλ5592 and O V$\lambda\lambda\lambda$5598, 5604, 5608) is always variable (about 3–7% of the adjacent continuum flux), with a burst (9–10% variability) of emission occuring on the 1998 January run;
4. The He Iλ5876 stellar emission feature generally exhibits variability from 4–12%, up to about 17% of the continuum flux on 1998 January 21. Note that the variability in this line is dominated by its P-Cygni absorption component. However, the emission component variability is clearly detected on 1996 January 15, 1996 May 26, 1996 July 28, 1996 September 30, 1996 November 16, and 1996 November 17;
5. The stellar complex C IV$\lambda\lambda$5801/12+C IIIλ5826 is always variable with amplitudes reaching 6–13% of the continuum flux, and sometimes up to 17%. Note that the entire line shows prominent variability (although marginally detected during the 1997 March run because of poor S/N ratio), suggesting blobs/inhomogeneities propagating into the whole line emission region;
6. The C IIIλ5696 stellar line always shows significant variability of 10–17% of the continuum flux, the maximum (≈29%) being detected on 1998 January 21 and correlated with bursts of C IV$\lambda\lambda$5801/12+C IIIλ5826, He Iλ5876 and the oxygen complex at ≈5590 Å. Note that like the C IV$\lambda\lambda$5801/12+C IIIλ5826 emission lines, the entire C III line shows prominent variability. On the whole, the 1998 January run appears as a particular epoch of high activity for this central star;
7. As was already noticed for massive WR stars (Robert 1992) and the low-mass [WC 9] star BD +30°3639 (Grosdidier et al.; Paper I), the blue-shifted absorption component of the lines exhibiting P-Cygni profiles in

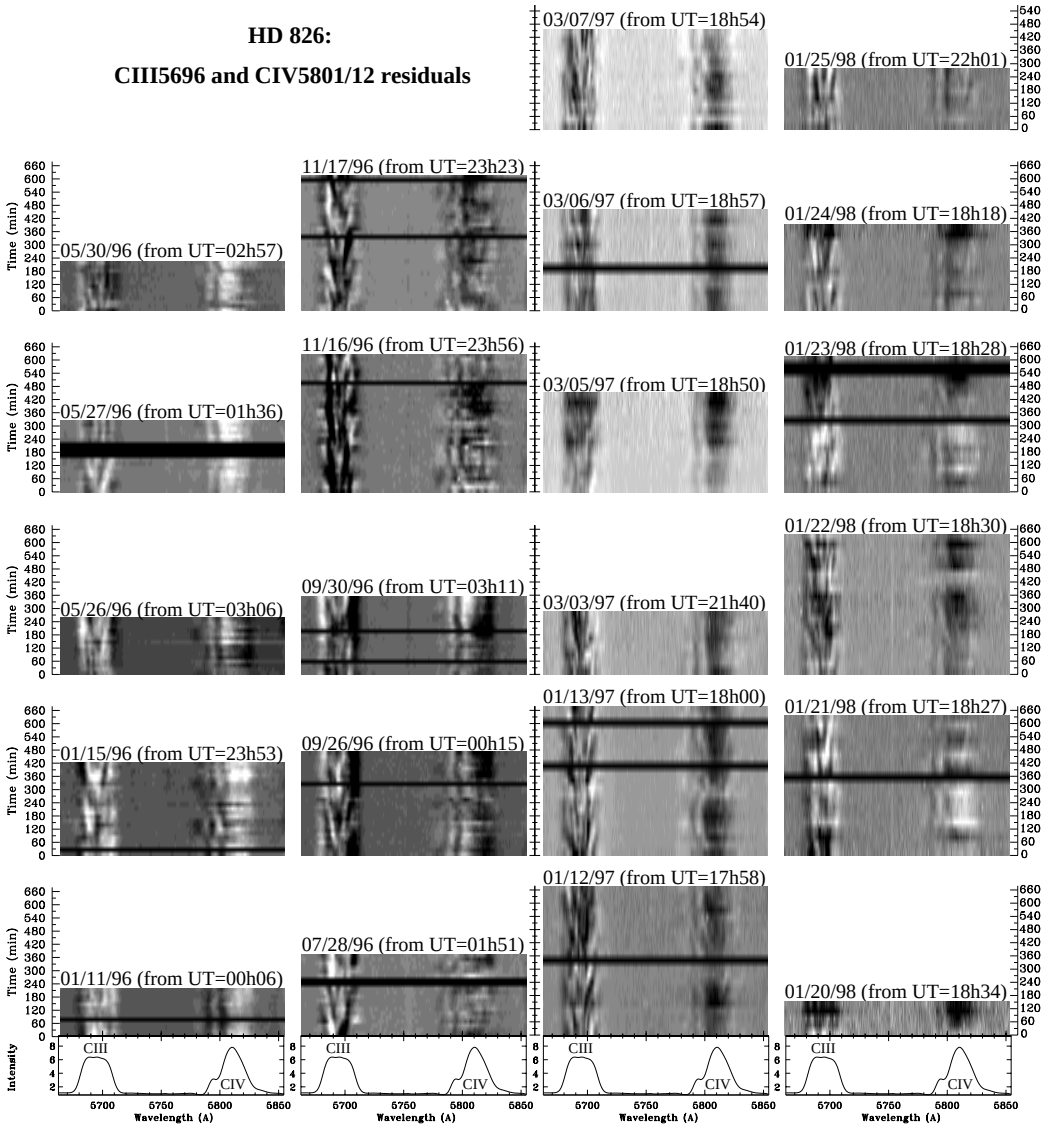

Fig. 3. Grayscale plots for HD 826 of C IIIλ5696 & C IV$\lambda\lambda$5801/12 residuals for 22 nights. Bottom panels show the 22-night mean. The range of the grayscale plots is −1.0 (black, lack of emission) to 1.0 (white, excess of emission) continuum units

HD 826 is significantly more variable than the emission component. This is likely mainly due to the small volume of matter in front of the stellar "disk", making it more sensitive to relative fluctuations.

Note that the variability of the He Iλ5876 *nebular* line centred on the broad emission is illusory. It is caused by imperfect guiding and variable seeing (typically 2–3″), both of which remove stellar light but not nebular light from the slit, in combination with rectification of the stellar continuum to unity. This effect appears only marginally for the [N II]λ5755 nebular line. The nebular line raw data show no significant variability.

3.3. Kinematics of the C IIIλ5696 subpeaks

The clearly visible C IIIλ5696 subpeaks always show measurable velocity shifts during their lifetime. Given the typical error in measuring the radial velocity (about 10–40 km s^{-1}) the trajectories of the subpeaks (or gaps) appear virtually related to features accelerating at an apparently *constant* acceleration. Thus, for the *intense* features (representing an apparent excess of emission as well as an apparent deficit of emission in the difference spectra) seen on at least three consecutive spectra, we measured mean radial velocities $v_{\rm R}$ and computed the related mean radial accelerations $a_{\rm R} = {\rm d}v_{\rm R}/{\rm d}t$ through *linear* fits. Figure 6 summarizes the results for 120 extracted features. Horizontal error bars reflect the observed *range* of radial velocities for a single blob, whereas vertical error bars show the range ($\pm 1\sigma$) of possible accelerations derived from the linear fits. The spread in $v_{\rm R}$ values suggests that the starting and ending wavelengths appear at random. In contrast with Balick et al. (1996), we report a significant spread in the apparent acceleration values.

The distribution does not appear symmetric in each of the two occupied quadrants, a few blobs with significant higher acceleration being observed in the wind receding

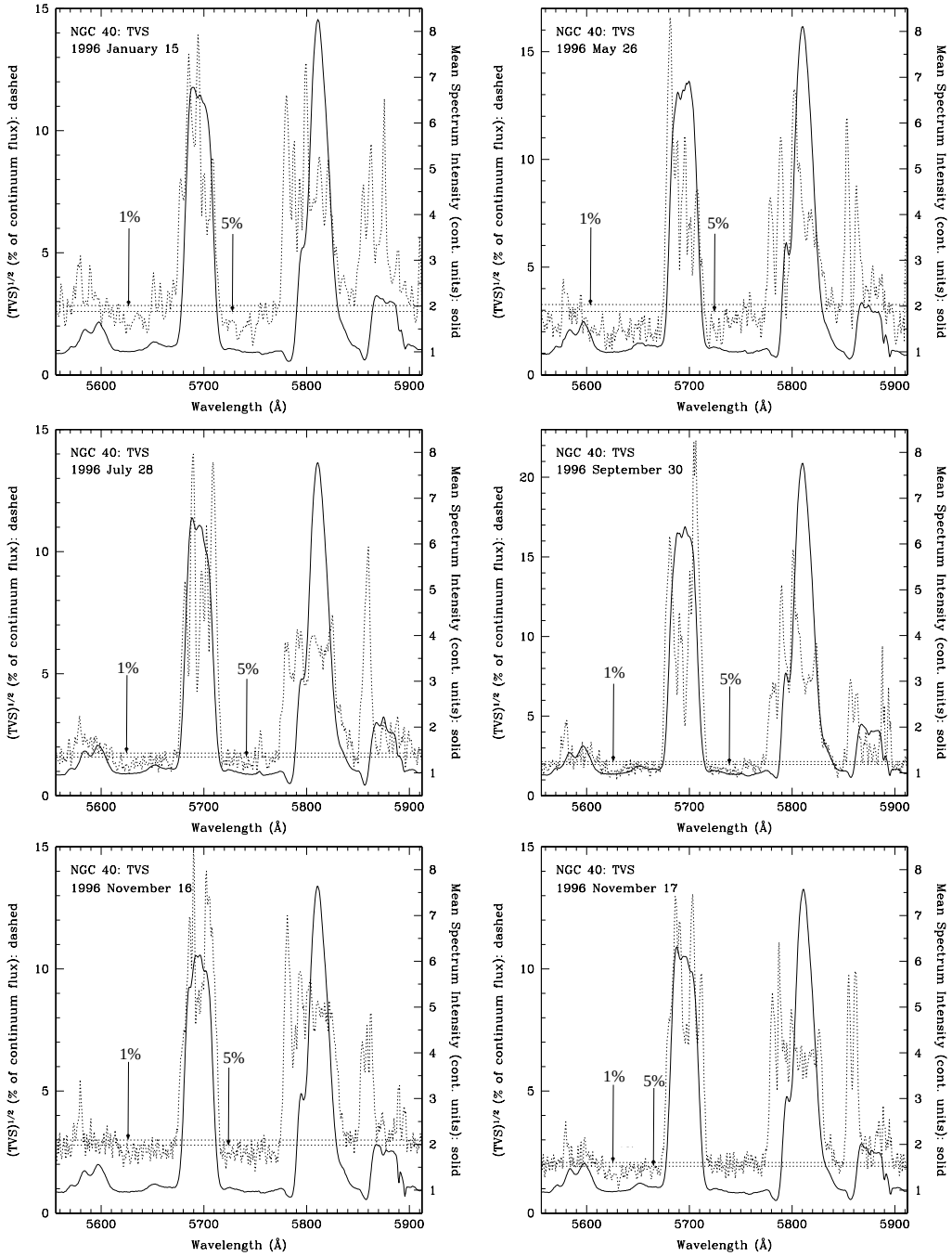

Fig. 4. HD 826 nightly mean spectra (solid lines) and the computed square root of the TVSs (dashed curves), for 6 nights (see text). Contours of statistical significance for 1% and 5% levels are indicated by *horizontal* dotted lines (see arrows). Our calculations account for pixel-to-pixel and spectrum-to-spectrum differences in the noise distribution

region. We suspect that, if more blobs had been secured for a larger sample of spectra, the distribution would have been more symmetric. Therefore, we interpret this fact as a statistical effect. As already noticed for BD +30°3639 (Paper I), the large majority of the blobs in Fig. 6 satisfies $a_{\rm R} \times v_{\rm R} \geq 0$. Therefore, the assumption of *outwardly* radially accelerating features is quite reasonable. However, 4 structures (only two at more than 2σ) move towards line centre. These features are likely spurious, being the tail end of a statistical distribution.

For comparison, the theoretical $(a_{\rm R}, v_{\rm R})$-relation derived from the β velocity field, $v(r) = v_\infty(1 - R_*/r)^\beta$, is also plotted in Fig. 6 for different angles θ between the line of sight and blob directions of movement ($v_{\rm R} = v(r)\cos\theta$, $a_{\rm R} = {\rm d}v_{\rm R}/{\rm d}t$). Adopting $v_\infty = 1000$ km s^{-1} and the value $R_* = 0.33\ R_\odot$ for HD 826 (Leuenhagen et al. 1996), the kinematics are consistent with a β velocity law with $\beta \approx 10$, in contrast to the value $\beta = 1$ adopted in the atmosphere model (Leuenhagen et al. 1996). A β value as small as 1 is ruled out because it would imply accelerations

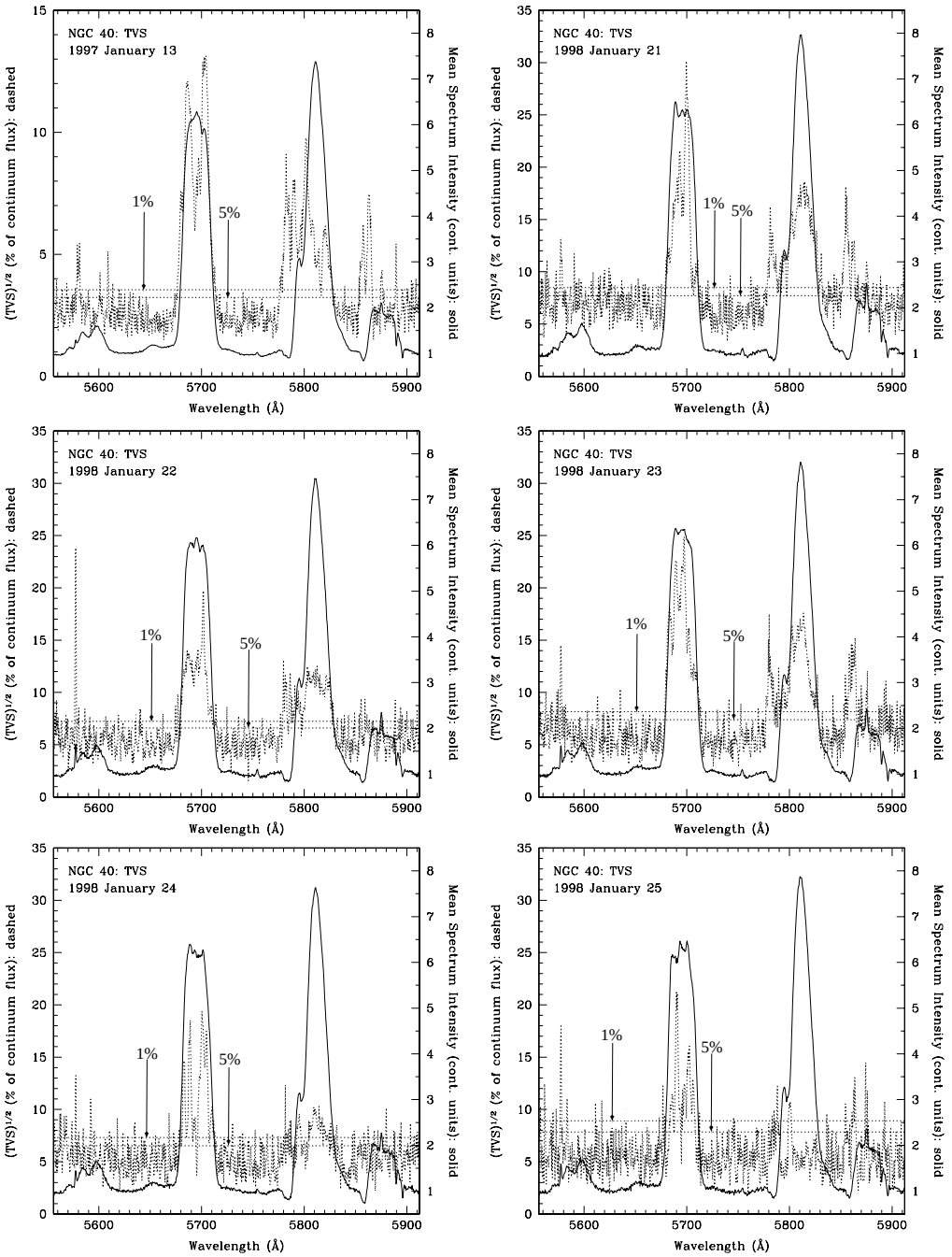

Fig. 5. HD 826 nightly mean spectra (solid lines) and the computed square root of the TVSs (dashed curves), for 6 other nights (see text and Fig. 4)

ranging up to about 0.65 km s^{-2}, which are not observed (see also Sect. 3.2.4 of Paper I). The line formation region is evaluated to span radial distances 10–100 R_* from the nucleus, judging from the distribution of the data in Fig. 6. Therefore, the line formation region appears much more extended than previously reported by Balick et al. (1996). Since the lifetime of the subpeaks is a few hours, they would cross, at speed $\lessapprox$1000 km s^{-1}, a zone limited to about a few tenths of the line formation region in radial extension. Thus the wind of HD 826 is highly variable on a very short time-scale, which supports a turbulent origin. Note that Lépine et al. (2000) find lifetimes for C IIIλ5696 blobs in the wind of the pop. I WC 8 star WR 135 to be of the order of the crossing time in the C IIIλ5696 formation zone, thus implying relatively long lasting blobs, that still could be turbulent.

Judging from the distribution of the data in Fig. 6, we estimate βR_* for HD 826 to be around 3.3 $R_\odot$. For nine massive WR stars, Lépine & Moffat (1999) found $\beta R_* \gtrapprox 20$. Our lower βR_* is likely mainly related to the very small radius of HD 826, as expected for PN nuclei.

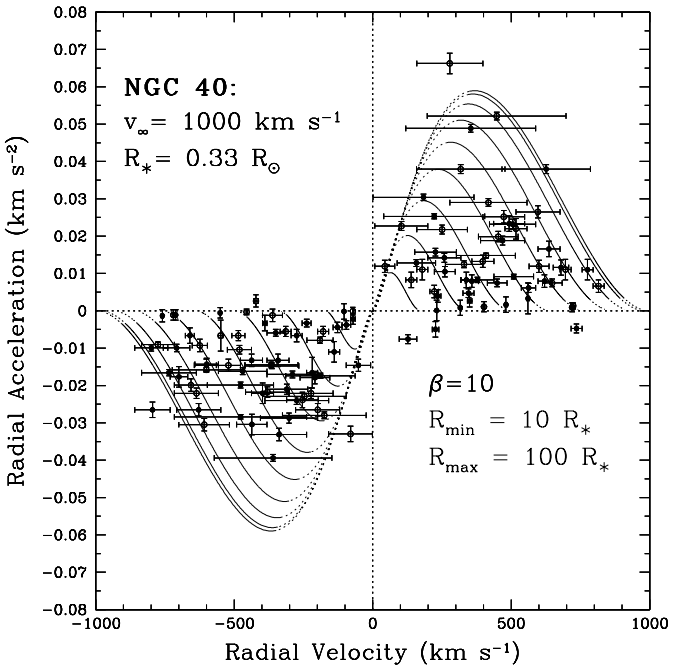

Fig. 6. Kinematics in the form of projected mean acceleration vs projected mean velocity for each subpeak/gap on top of the C IIIλ5696 emission line (120 points). Filled (open) symbols correspond to an excess (deficit) of emission. The projected β-velocity law is shown for $\theta = 0°$ (towards the observer, lower left corner) to 180° (away from the observer, upper right corner), in steps of 10° ($R_{\min} \leq r \leq R_{\max}$: solid curves; $r < R_{\min}$ and $r > R_{\max}$: dotted lines). We use the stellar parameters given by Leuenhagen et al. (1996); see text

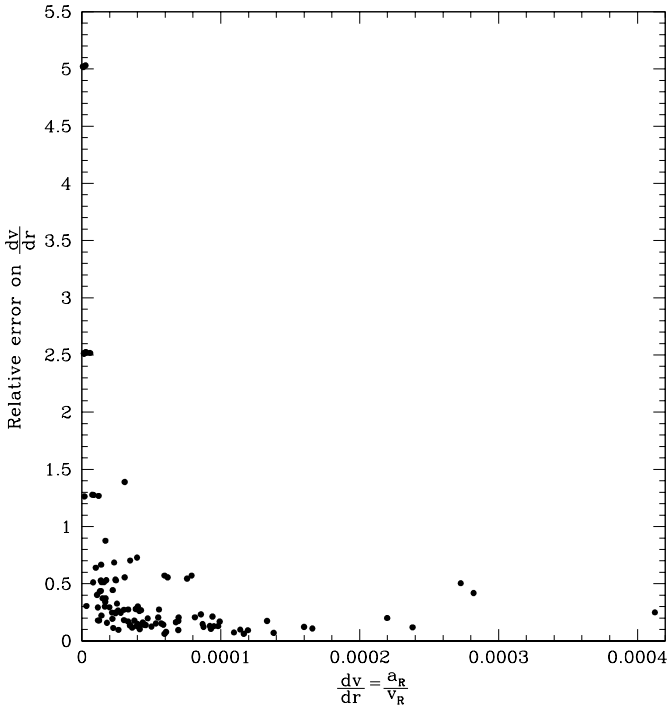

Fig. 7. Relative error on $\mathrm{d}v/\mathrm{d}r$, $\sigma(\mathrm{d}v/\mathrm{d}r)/(\mathrm{d}v/\mathrm{d}r)$, as a function of $\mathrm{d}v/\mathrm{d}r$ for the blobs in Fig. 6, satisfying $a_{\mathrm{R}} \times v_{\mathrm{R}} \geq 0$. The horizontal axis is in s^{-1}

Recall that the expected maximum acceleration within a β-velocity field is proportional to $k(\beta)v_\infty^2/R_*$, with the function k (see Paper I) being only slightly dependent on β for β above 2–3. Thus, fitting the observed maximum acceleration with the theoretical $(a_{\mathrm{R}}, v_{\mathrm{R}})$-relation gives a constraint on the ratio v_∞^2/R_*. Therefore, we expect that reliable values on v_∞ and R_* should follow the relation: $v_\infty^2/R_* \sim$ 4–5 km s^{-2}.

Absolute values of the acceleration in Fig. 6 range from nearly 0 to 70 m s^{-2}. The mean radial acceleration in the line formation zone (calculated from the 120 observed points) is 14.7 ± 11.7 m s^{-2} (compared to only 3.6 ± 0.8 m s^{-2} for BD +30°3639; Paper I). Within the line formation region, the spread in acceleration values appears quite large. Overall, these values in HD 826 are very similar to those observed in the massive WC 8 star WR 135 (Robert 1992; Lépine & Moffat 1999). However, especially impressive are the 3–4 times larger observed maximum a_{R} values (HD 826: $\approx$66 m s^{-2}) compared to those already reported for massive WC 5–9 stars or low-mass [WC 9] stars (4–20 m s^{-2}: see Paper I; Lépine & Moffat 1999; Robert 1992). Note that in massive WR stars the amplitudes of the accelerations do not show correlations with either the stellar effective temperature, or the stellar luminosity (see Table 4 in Lépine & Moffat 1999). Thus, conjecturing that this property still holds for low-mass WR stars, and although HD 826's massive counterparts have larger terminal velocities, large maximum a_{R} values are mainly a consequence of its very small core radius.

3.4. The velocity gradient in the line formation region

We have considered the whole set of blobs satisfying $a_{\mathrm{R}} \times v_{\mathrm{R}} \geq 0$, and calculated all their related corresponding $a_{\mathrm{R}}/v_{\mathrm{R}} = \mathrm{d}v/\mathrm{d}r$. Note that the relative error on $\mathrm{d}v/\mathrm{d}r$ is often quite large: see Fig. 7. However, the relatively high number of subpeaks encouraged us to perform a statistical analysis of the $\mathrm{d}v/\mathrm{d}r$ derived from our kinematic measurements. Figure 8 shows the frequency distribution of the $\mathrm{d}v/\mathrm{d}r$ values (solid histogram). Large bins have been chosen in order to compensate for the errors encountered in evaluating the $\mathrm{d}v/\mathrm{d}r$. For comparison, the distribution expected from a purely β velocity field is also shown (dotted histogram), for the radial distances between $R_{\min} = 10\ R_*$ and $R_{\max} = 100\ R_*$ found before, assuming $\beta = 10$, $R_* = 0.33\ R_\odot$, and $v_\infty = 1000$ km s^{-1}. The latter histogram has been normalized to the observed histogram at their maxima, occurring in the same bin. Note the huge excess of features occurring at $\mathrm{d}v/\mathrm{d}r > 2\ 10^{-5}$ s^{-1}, compared to the number expected from a pure β-velocity field. Since the majority of the features showing $\mathrm{d}v/\mathrm{d}r$ above $2\ 10^{-5}$ s^{-1} have relative errors $\lesssim$30%, this result appears to be reliable. This suggests that the β velocity field underestimates the true gradient within the flow. Such a result has been also established in Paper I for the [WC 9] nucleus BD +30°3639. This is in line with other studies

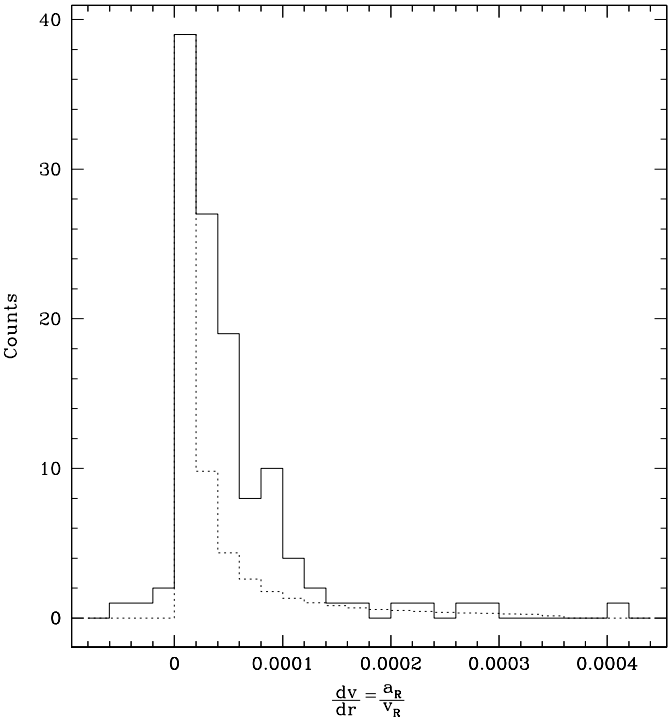

Fig. 8. Frequency distribution of the dv/dr values (solid histogram). For comparison, the distribution expected from a true β-velocity field is also plotted (dotted histogram). The line formation region in the second histogram is assumed to span radial distances 10–100 R_* from the central star, with $\beta = 10$ (see text). The horizontal axis is in s^{-1}

concerning the high efficiency of the acceleration in the optically thin regions of pop. I WR winds (Marchenko & Moffat 1999).

4. Discussion and conclusion

In the present paper, we have seen that the star HD 826 shows temporal changes in the shapes of its C IIIλ5696 and C IV$\lambda\lambda$5801/12+C IIIλ5826 emission lines. The amplitudes of the variations range up to 25–30% of the adjacent continuum flux, over timescales of hours. The variabilities of both lines are quite well correlated, although they are somewhat weaker for the C IV complex. On the whole, the 1998 January run appears as a particular epoch of high activity for this central star.

As was already noticed for massive WR stars, the blue-shifted absorption component of the lines exhibiting P-Cygni profiles in HD 826 is significantly more variable than the emission component. This is likely mainly due to the small volume of matter in front of the stellar "disk", a large fraction of which is subject to a higher level of coherent variability. This suggests linear sizes for the blobs of $\sim$1 R_*.

The subpeaks show large measurable velocity shifts in HD 826 during their lifetime. Subpeaks (or gaps) on the top of the C III line generally move from about the line center towards line edges in a symmetric fashion. This is consistent with wind features accelerated outward along radial trajectories. Since the lifetime of the subpeaks is a few hours, they cross, at speed $\lesssim$1000 km s^{-1}, a zone limited to about a few tenths or less of the line formation region in radial extension. Thus the wind of HD 826 is highly variable on a very short time-scale, which supports a turbulent origin.

The kinematics of 120 structures on top of the C IIIλ5696 line of HD 826 have been measured. Adopting $v_\infty = 1000$ km s^{-1} and $R_* = 0.33\ R_\odot$ the kinematics are well reproduced by a β-velocity law with $\beta \approx 10$, in contrast with the value $\beta = 1$ adopted in the atmosphere model. The line formation region is evaluated to span radial distances 10–100 R_* from the central star. Within the accuracy of our acceleration measurements, $R_* = 0.33\ R_\odot$ and $\beta = 10$ (hence $\beta R_* \approx 3.3$) seem to be good estimates of the stellar radius and of the β parameter. Keeping $\beta = 1$ and fitting the observed maximum acceleration with the theoretical (a_R, v_R)-relation would require a downward revision of the ratio v_∞^2/R_* by a factor $\approx$10. Because of the quite good reliability of the terminal velocity estimate ($\approx$1000 km s^{-1}), keeping $\beta = 1$ would therefore imply rather high, unrealistic values of the stellar radius (3.3–3.6 $R_\odot$). Therefore we reject a β value of 1 in favor of $\beta \approx 10$, which is consistent with previous estimates of β for massive WR stars given in Moffat (1996).

The line variability in HD 826 is somewhat similar to that observed in the massive WC 8 star WR 135 (see Robert 1992; Lépine & Moffat 1999; Lépine et al. 2000). Thus, on the whole, the wind fragmentation process appears to be a purely atmospheric phenomenon, despite the strong differences between both types of underlying hot star. However, some differences exist: i) in the complex C IV$\lambda\lambda$5801/12+C IIIλ5826 emission line originating in HD 826, moving subpeaks appear with adjacent ghost images. This is likely due to line blending. Unfortunately, this blending prevented us from clearly identifying moving features. This was not the case for WR 135 (see Lépine et al. 2000); ii) in addition, Lépine et al. (2000) find lifetimes for C IIIλ5696 blobs in the wind of WR 135 to be of the order of the crossing time in the C IIIλ5696 formation zone, thus implying relatively *long*-lasting blobs, compared to those observed in HD 826.

Combining the results of Paper I with those of the present paper we find that [WC 9] and [WC 8] central stars exhibit similar changes in their C IIIλ5696 and C IV$\lambda\lambda$5801/12+C IIIλ5826 emissions. We therefore suspect that, if more data had been secured for a larger sample of late subtype [WC] stars, the phenomenon of emission line variability in central stars might have revealed itself to be more common and universal. However, the details differ. For example, accelerations exhibited by the clumps originating in HD 826 are often significantly larger than those in BD +30°3639 or massive WR stars. This difference could be understood by the smaller hydrostatic radius of HD 826. However, it will be important in the near future to test whether the data indicate any true

correlation of the observed variations of the emission lines with radius or any other fundamental stellar parameters, for a larger sample of stars. In the case of pop. I WR stars, no such correlation is seen (Lépine & Moffat 1999).

Finally, high resolution ($\leq$0.5 Å), high S/N ratio, temporally resolved, optical spectra of HD 826 are needed in order to investigate the appearance and dynamics of subpeaks observed so far at inferior resolutions. In particular, the possible hierarchy of subpeaks within each individual subpeak (such a fractal-like structure is expected in the context of supersonic, compressible turbulence) could be tested in this way. For that purpose, the need for large, 10 m-class telescopes is critical.

Acknowledgements. YG acknowledges financial aid from the French Ministry of Foreign Affairs. AFJM is grateful to NSERC (Canada) and FCAR (Québec) for financial support. AFJM acknowledges the award of a Killam Fellowship from the Canada Council for the Arts. We thank Thomas Eversberg for his help in the data acquisition (OMM data).

References

Acker, A., Górny, S. K., & Cuisinier, F. 1996, A&A, 305, 944
Acker, A., Grosdidier, Y., & Durand, S. 1997, A&A, 317, L51
Acker, A., Marcout, J., Ochsenbein, F., Stenholm, B., & Tylenda, R. 1992, The Strasbourg-ESO Catalogue of Galactic Planetary Nebulae, European Southern Observatory, Garching
Balick, B., Rodgers, B., Hajian, A., Terzian, Y., & Bianchi, L. 1996, AJ, 111, 834
Benvenuti, P., Perinotto, M., & Willis, A. J. 1982, in IAU Symp. 99, Wolf-Rayet Stars: Observations, Physics, Evolution, ed. C. W. H. de Loore, & A. J. Willis (Dordrecht: Reidel), 453
Bianchi, L. 1992, A&A, 253, 447
Bianchi, L., & Grewing, M. 1987, A&A, 181, 85
Crawford, I. A., & Barlow, M. J. 1991, A&A, 249, 518
Eversberg, T., Lépine, S., & Moffat, A. F. J. 1998, ApJ, 494, 799
Fullerton, A. W., Gies, D. R., & Bolton, C. T. 1996, ApJS, 103, 475
Gillet, D., Burnage, R., Kholer, D., et al. 1994, A&AS, 108, 181
Górny, S. K., & Stasińska, G. 1995, A&A, 303, 893
Grosdidier, Y., Acker, A., & Moffat, A. F. J. 2000, A&A, 364, 597, Paper I
Grosdidier, Y., Acker, A., Moffat, A. F. J., Chesneau, O. & Dimeo, T. 1997, in IAU Symp. 180, Planetary Nebulae, ed. H. J. Habing, & H. J. G. L. M. Lamers (Dordrecht: Reidel), 108
Hu, J. Y. & Bibo, E. A. 1990, A&A, 234, 435
van der Hucht, K. A. 1996, Ap&SS, 238, 1
van der Hucht, K. A. 1999, in IAU Symp. 193, Wolf-Rayet Phenomena in Massive Stars and Starburst Galaxies, ed. K. A. van der Hucht, G. Koenigsberger, & P. R. J. Eenens, San Francisco, Calif.: Astronomical Society of the Pacific, 13
Köppen, J., & Tarafdar, S. 1978, A&A, 69, 363
Lépine, S., & Moffat, A. F. J. 1999, ApJ, 514, 909
Lépine, S., et al. 2000, ApJ, 120, 3201
Leuenhagen, U., Hamann, W.-R., & Jeffery, C. S. 1996, A&A, 312, 167
Marchenko, S. V., & Moffat, A. F. J. 1999, A&A, 341, 211
Meaburn, J., Lopez, A., Bryce, M., & Mellema, G. 1996, A&A, 307, 579
Méndez, R. H., & Niemela, V. S. 1982, IAU Symp. 99, Wolf-Rayet Stars, ed. C. W. H. de Loore, & A. J. Willis, 457
Moffat, A. F. J. 1996, in Wolf-Rayet Stars in the Framework of Stellar Evolution, Proc. 33rd Liège International Colloq., ed. J. M. Vreux, A. Detal, D. Fraipont-Caro, E. Gosset, & G. Rauw, Liège: Univ. Liège, Inst. d'Astrophys., 199
Neiner, C., Acker, A., Gesicki, K., & Sczerba, R. 2000, A&A, 358, 321
Peña, M., Stasińska, G., Esteban, C., et al. 1998, A&A, 337, 866
Pottasch, S. R. 1996, Ap&SS, 238, 17
Robert, C. 1992, Ph.D. Thesis, Université de Montréal, Canada
Schmutz, W., Hamann, W.-R., & Wessolowski, U. 1989, A&A, 210, 236
Tylenda, R., Acker, A., & Stenholm, B. 1993, A&AS, 102, 595